Automatic Classification and Differentiation of Atherosclerotic Lesions in Swine Using IVUS and Texture Features

P Brathwaite, A Nagaraj*, B Kane*, DD McPherson*, EL Dove

The University of Iowa, Iowa City, Iowa, USA

Northwestern University*, Chicago, Illinois, USA

Abstract

Our goal was to develop an automatic classification algorithm to differentiate between four common lesion types in atherosclerotic (AS) arteries: calcific (CAL), fibro-calcific (FBC), fibrous (FBR), and fibro-fatty (FBF). AS was induced in eight Yucatan miniswine. 22 femoral or carotid arteries were imaged with intra-vascular ultrasound using a pull-back procedure. Both 2D ad 3D texture measures were used, followed by a principal components analysis to reduce dimension. The classifiers were applied to the test dataset, and the results were compared with two independent experts. There was no difference between the 2D and 3D classification of the CA and E1, and of the CA and E2 (ANOVA, F=2.00). The difference between CA and E1 (or E2) was not larger than the difference between E1 and E2 for any lesion type (ANOVA, F=0.76). We conclude that using 3D information in the classification scheme improved the algorithm's ability to correctly classify lesion type.

1. Introduction

Atherosclerosis is a disease that affects people of any age and is characterized by the narrowing of arteries due to the progressive thickening of deposits within the lining of the arterial wall. It is the leading cause of death in the western world, and is predicted to continue to be the leading cause of death within the first quarter of the next century. It is estimated to cost over $100 billion dollars annually in health care [3].

It is often difficult for clinicians to accurately determine the type and morphology of the atherosclerotic plaque or lesion within an arterial wall. This is especially so for fibrous and fibro-calcific lesions [2]. Our goal was to develop an automatic classification scheme to differentiate between four types of atherosclerotic lesions: calcified (CAL), fibro-calcific (FBC), fibrous (FBR), and fibro-fatty (FBF).

Conventional methods such as planar angiography and X-ray are not capable of describing the different types of lesions present in the artery. Modern magnetic resonance imaging has had some success at discriminating the components of the lesions; however structural resolution is presently not good enough to visualize the extent and composition of atherosclerotic plaques, especially in coronary arteries. Electron-beam computed tomography is highly sensitive in detecting coronary artery calcification in comparison with other modalities, but it is limited to the detection of calcific plaques. Optical coherence tomography (OCT) has an advantage over other modalities in that it can image components of plaque at a resolution that other modalities cannot achieve, but it is not widespread in its clinical use. It also has a limited depth of penetration so although it may provide excellent images, it doesn't give information about deeper structures. Structures deep within arterial walls can best be visualized by intravascular ultrasound (IVUS).

2. Methods

2.1. Animal preparation and data collection

Animal (Yucatan miniswine pigs) experiments, undertaken at Northwestern University, Chicago, Illinois, involved two series of studies. In one series, the animals underwent an initial surgical procedure to place markers on the carotid and iliofemoral arteries. The animals were then allowed to recover and fed a hypercholesterolemic diet for 12 months. After 12 months the animal underwent a terminal surgical study during which time IVUS images were acquired. In a second series both carotid and iliofemoral arteries were exposed and markers placed under initial sterile surgery. The animals underwent percutaneous angioplasty to denude the endothelium of one carotid and one iliofemoral artery chosen randomly. This allowed active plaque development consisting of fatty, fibrous and subsequent fibrocalcific components. Following surgery the hypercholesterol diet regimen continued and the animals were evaluated at different times during the study.

Pull-back sequences of two-dimensional (2D) IVUS images of twenty-two (22) highly diseased arteries were

single lesion type identified by an expert that is three-dimensionally connected. For complex lesions comprised of more than one lesion type, the individual lesion components were separated and considered as separate lesions.

Some IVUS images of the arteries were acquired 1 year after the start of the experiment where the pigs were fed a high-fat diet with no prior arterial denudation, while other IVUS images of the arteries were obtained 2 months after the start of the same diet regimen, but with prior arterial denudation. An average of twenty-one (21) physical image slices were acquired of each artery at 1 mm intervals using an UltraCross 30 MHz Coronary Imaging Catheter (3.2F or 5F) from Boston Scientific SciMed, Maple Grove, MN. The constant velocity pull-back rate was 0.5 mm/s and the image resolution was 0.1 mm in the axial and lateral directions. Image slice thickness was 1 mm in the axial direction. At each physical slice, images was acquired at the *q*, *s*, *i* and *t* points of the EKG cycle resulting in an average total of 84 time slices per artery. The *i* point in the EKG cycle was defined as the equi-potential point, i.e. just after the QRS complex where the potential returns to its original level (pre-QRS level). Image slices were arranged in the same *q*, *s*, *i* and *t* sequence from the first image slice acquisition to the end of the pull-back sequence, prior to application of the texture measures.

The images were randomly divided into a training set (8 arteries), and a test set (14 arteries) to develop (test set) and test (training set) the performance of the automatic classification algorithm. The number of arterial lesions in each set is shown in Table 1. The classifiers were based either on two-dimensional (2D) or three-dimensional (3D) calculations.

Table 1 – Number of lesion types in the training and test sets from 22 arteries

DATA SET	CAL	FBC	FBR	FBF	TOTAL
2D TRAIN	4	18	13	15	50
2D TEST	7	20	16	5	48
3D TRAIN	0	6	10	7	23
3D TEST	3	13	10	3	29

2.2. Classification algorithms

The following texture features were used to applied to the segmented lesions [6] -- First-order statistics: mean, variance, skewness, kurtosis; Second-order statistics: short run emphasis, long run emphasis, gray level non-uniformity, runlength non-uniformity, run percentage; distance *d* along a direction ϕ): angular second moment, contrast, correlation, co-occurrence variance, inverse difference moment, sum average, sum entropy, sum variance, entropy difference, variance difference, entropy information measure of correlation 1, information measure of correlation 2, maximum probability.

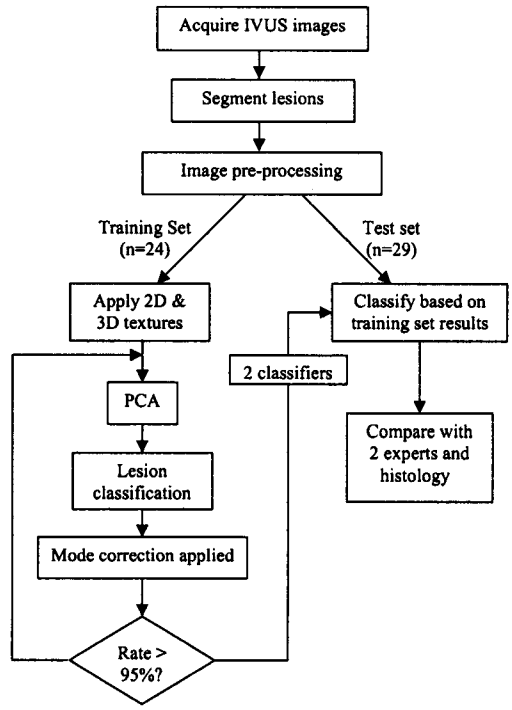

Figure 1 – Experimental Methods Flowchart.

Principal components analysis (PCA) was then used to determine the best combination of variables that would account for at least 95% of the variation in the texture variables [6]. PCA involves the selection of a set of weights such that the variance of the linear composite is a maximum. The goal is to choose a small number of linear composites that would provide 95% of the information residing in the larger set of original texture variables. PCA produces an orthogonal coordinate system in which the axes are ordered in terms of the amount of variance in the original data for which the corresponding principal components account. If the first few principal components account for most of the variation, then the dimensionality of the problem is reduced and the texture variables with the highest discriminatory power to distinguish between the four types of lesions are found.

The classification algorithm was applied to both the standard 2D texture measures (2D classifier) and 3D texture measures (3D classifier) based on a new way of calculating the co-occurrence matrix. In the 3D case, the

computed from the new co-occurrence matrix.

2D and 3D textures measures were computed for all of the lesions in the training set and the resulting values submitted to the PCA procedure. Thus after applying the PCA procedure, redundancy and complexity were reduced by reducing the dimension space to seven. As a consequence, the PCA provided a smaller relevant set of texture measures that contained the most discriminatory information between lesion types. **Figure 1** illustrates the data analysis procedure.

2.3. Statistical analysis

To evaluate the performance of the classifiers, we compared the classifiers outputs with the 2 independent experts' classifications. Inter-operator variability was determined to assess whether the classifiers performance was as good as the difference between the two independent experts. The statistical comparison involved computing Kappa statistics, and performing a one-way analysis of variance (ANOVA) (level of significance of $\alpha = 0.05$) between the 2 classifiers, the 2 experts. To further demonstrate the performance of the classifiers, confusion matrices were tabulated [5]. Confusion matrices contain information about actual and predicted classifications performed by a classification system. It shows not only how well the model predicts, but also presents the details needed to see exactly where things may have gone wrong.

Kappa is a measure of agreement between observers. It compares the agreement against that which might be expected by chance. If there is complete agreement, then $\kappa = 1$. If observed agreement is greater than or equal to chance agreement, $\kappa \geq 0$, and if observed agreement is less than or equal to chance agreement, $\kappa \leq 0$ [5].

3. Results

There was no difference between the 2D and 3D classification of the computer algorithm (CA) and the first expert (E1), and of the CA and the second expert (E2 - ANOVA, F=2.00).

Table 2 – Confusion matrix for Expert 1 and Expert 2. The lesion types are fibro-fatty (FBF), fibrous (FBR), fibro-calcific (FBC), and calcified (CAL).

	Exp1			
Exp2	FBF	FBR	FBC	CAL
FBF	5	0	0	0
FBR	4	11	1	0
FBC	1	8	11	0
CAL	0	0	7	0

The difference between CA and E1 (or E2) was not increased when using the 3D CA (0.94, 0.81-1.06). Similar results were found when comparing CA with E1.

Table 2 shows the results (displayed as a confusion matrix) obtained from both experts. The data indicate that there was good agreement for FBF lesions, but there was some disagreement about the classification of FBR and FBF lesions, and FBC and CAL lesions.

Table 3 – Confusion matrix for 3D classifier comparing the classifications from the computer algorithm (CA) and the first expert (Exp1).

	Exp1			
CA	FBF	FBR	FBC	CAL
FBF	3	0	0	0
FBR	1	12	1	0
FBC	0	3	8	0
CAL	0	0	1	0

Table 4 – Confusion matrix for 3D classifier comparing the classifications from the computer algorithm (CA) and the first expert (Exp2).

	Exp2			
CA	FBF	FBR	FBC	CAL
FBF	3	0	0	0
FBR	0	10	4	0
FBC	0	0	9	2
CAL	0	0	0	1

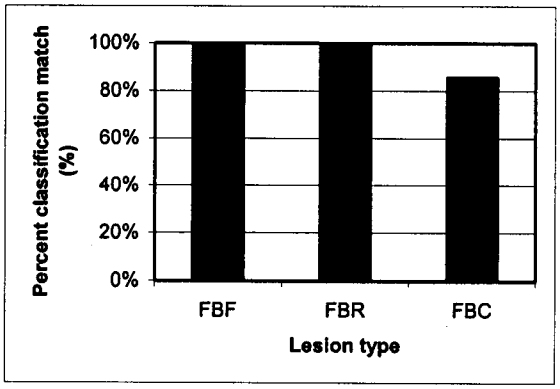

Figure 2 - Percent classification match for each lesion type in the 3D test set for the 3D classifier (COMP), where both experts agreed on the lesion type.

Table 3 shows a comparison of the results obtained from the computer–based 3D classification algorithm with the results of the classification of the first expert. Table 4 shows the same comparison but with the second expert.

4. Conclusions

We conclude that using 3D information in the classification scheme improved the algorithm's ability to correctly classify lesion type. The CA was able to correctly differentiate between FBR and FBC. Kappa statistics indicate moderate agreement for both classifiers versus either of the two experts. Mean values for the 3D classifier [0.36 - 0.68] were slightly higher than the 2D classifier [0.27 - 0.61]. This indicates slightly more agreement between the 3D classifier and the two experts and a better classification performance by the 3D classifier. The one-way ANOVA test for both classifiers indicated no statistical difference ($p > 0.05$) for the 3D classifier versus the experts, while there was a statistical difference between the 2D classifier and the experts. This means that classifications by the 3D classifier would be no different from those by either expert, while the 2D classifier would produce significantly different lesion classifications when compared to the experts.

The tabulated confusion matrices and their associated plots for the 3D classifier show the percent classification matches for the classifiers versus each expert within each lesion type for the test sets. We desire to have the classifier classifications match the expert classifications which would be represented by a diagonal confusion matrix (all zeros in the off-diagonal entries). However, it was more reasonable to expect a large number of lesion matches along the diagonal compared with the total number of lesions in each lesion type and a smaller number of mismatches off the diagonal. Overall, we observed that the experts had < 60% classification match for each lesion type for all the lesions in the test set with each other, but if we only tabulated percent classification match when the experts agreed, the rate was > 91% for the 2D classifier and >86% for the 3D classifier. Overall the confusion matrices and plots of the classifiers versus the experts indicated that they compared favorably.

We have developed a method of classifying the entire 3D lesion based on the individual 2D slices that compares favorably with two independent experts. Our method takes advantage of the spatial interdependencies along the length of the lesion by computing 3D co-occurrence texture measures from a new co-occurrence matrix and combining them with previously developed 2D texture measures to further improve the lesion classification rate. This method had smaller lesion classification error rates in comparison with the classifications from the 2D classifier. We need to be able to discriminate the lesion types into more categories that would assist a clinician's ability to prescribe the appropriate interventional or therapeutic procedure for the patient. We were able to discriminate between four lesions types and correlated well with the two independent experts with an independent lesion test set using a 3D classifier.

References

[1] Evans, JL, Ng K, Wiet SG, Vonesh M, Burns WB, Radvany M, Kane B, Davidson CJ, Roth SI, Kramer, BL, Meyers, SN and McPherson, DD. Accurate three-dimensional reconstruction of intravascular ultrasound data: Spatially correct three-dimensional reconstructions. *Circulation* 1996:93:567-576.

[2] McPherson DD. Three-dimensional arterial imaging, *Scientific-American: Science and Medicine*, 1996: 3(2):22-31.

[3] Mercuri M, McPherson DD, Bassiouny H and Glagov S. Non-Invasive Imaging of Atherosclerosis, Kluwer Academic Publishers, 1998.

[4] Mojsilović A, Popović M, Amoday N, Babić R and Ostojić M. Automatic segmentation of intravascular ultrasound images: A texture based approach, *Annals of Biomedical Engineering*, 1997:25:1059-1071.

[5] Schalkoff RJ. Pattern Recognition: Statistical, Structural and Neural Approaches, J. Wiley and Sons, New York, 1992.

[6] Sonka M, Hlavac V, and Boyle R. Image Processing, Analysis, and Machine Vision, PWS Publishing, 2nd Edition, 1998.

Address for correspondence.

Edwin L. Dove, Ph.D.
Department of Biomedical Engineering
The University of Iowa
Iowa City, Iowa 52242 USA
Edwin-Dove@uiowa.edu